Rossby-wave scales, propagation and the variability of eddy-driven jets

Elizabeth A. Barnes [*] and Dennis L. Hartmann

Department of Atmospheric Sciences, University of Washington, Seattle, Washington

---

[*] *Corresponding author address:* Elizabeth A. Barnes, Department of Atmospheric Sciences, University of Washington, Box 351640, Seattle, WA 98195.

E-mail: eabarnes@atmos.washington.edu

ABSTRACT

The eddy-driven jet is located in the midlatitudes, bounded on one side by the pole and often bounded on the opposite side by a strong Hadley-driven jet. This work explores how the eddy-driven jet and its variability persist within these limits. It is demonstrated in a barotropic model that as the jet is located at higher latitudes, the eddy-length scale increases as predicted by spherical Rossby-wave theory, and the leading mode of variability of the jet changes from a meridional shift to a pulse. Looking equatorward, a similar change in eddy-driven jet variability is observed when it is moved equatorward toward a constant subtropical jet. In both the poleward and equatorward limits, the change in variability from a shift to a pulse is due to the modulation of eddy propagation and momentum flux. Near the pole, the small value of beta and subsequent lack of wavebreaking near the pole accounts for the change in variability, whereas on the equatorward side of the jet, the strong subtropical winds can affect eddy propagation and restrict the movement of the eddy-driven jet or cause bimodal behavior of the jet latitude. Barotropic quasilinear theory thus suggests that the leading mode of zonal-wind variability will transition from a shift to a pulse as the eddy-driven jets move poleward with climate change, and that the eddy-length scale will increase as the jet moves poleward.

1. Introduction

The eddy-driven jet and its variability exist within the region between the pole and the Hadley-driven subtropical jet. While the leading mode of variability of the eddy-driven jet is often associated with a meridional shifting of the zonal-mean zonal winds, Eichelberger and Hartmann (2007) showed in a simple general circulation model that in the presence of a strong subtropical jet, the leading mode describes a pulsing of the eddy-driven jet. As the eddy-driven jet nears the pole its variability also changes from a shift to a pulse, with the persistence of the variability decreasing with jet latitude (Kidston and Gerber 2010; Barnes et al. 2010; Barnes and Hartmann 2010).

The goal of this work is to investigate one overarching question: "What are the equatorward and poleward constraints on eddy-driven jet variability?" More specifically, we will focus on the following questions:

- Why does the variability of the jet change from a shifting to a pulsing in the presence of a strong Hadley-driven jet in observations?
- Why does the variability of the jet change from a shifting to a pulsing as the eddy-driven jet is moved poleward in a barotropic model?
- How does the scale of the eddies change as the jet shifts poleward?
- How do changes in jet variability relate to changes in eddy-mean flow feedbacks and persistence?

To answer these questions, we employ a stochastically stirred barotropic model to mimic a midlatitude storm track. A barotropic model is a good vehicle for understanding annular mode variability because these modes require meridional transport of momentum by eddies as a fundamental process for their existence. Meridional wave propagation and wave mean-flow interaction theory are therefore central and well captured in a barotropic model. In this context, meridionally-confined stirring in a barotropic model is a reasonable analogue for a baroclinic storm track, since in both cases the generation of the eddies is maximum in the jet core, and it is the meridional fluxes into and out of the jet that are critical.

2. Methods

We follow Vallis et al. (2004) and Barnes et al. (2010) and integrate the spectral non-divergent barotropic vorticity equation on the sphere,

$$\frac{\partial \zeta}{\partial t} + \frac{u}{a\cos\theta}\frac{\partial \zeta}{\partial \lambda} + \frac{v}{a}\frac{\partial \zeta}{\partial \theta} + v\beta = \mathcal{S} - r\zeta - \kappa\nabla^4\zeta, \tag{1}$$

where r is the damping parameter set equal to 1/6 days^{-1} and κ is the diffusion coefficient for parameterizing the removal of enstrophy at small scales. The model is run at a resolution of T42 and atmospheric eddies are modeled as an Ornstein-Uhlenbeck stochastic process ($\mathcal{S}$) defined for each combination of total wavenumber l and zonal wavenumber m:

$$\mathcal{S}_{lm} = (1 - e^{2dt/\tau})^{1/2} Q^i + e^{-dt/\tau}\mathcal{S}_{lm}^{i-1}, \tag{2}$$

where τ denotes the decorrelation time of the stirring (2 days) and dt is the model time step (3600 seconds). Q^i is a real number chosen uniformally between $(-\mathcal{A}, \mathcal{A}) \times 10^{-11}$, where $\mathcal{A}$ is the stirring strength (see Vallis et al. (2004) for details). The model is stirred over a range of total wavenumbers, and the sensitivity of the results on the stirring scale will be discussed in detail in Section 3. Finally, to mimic a meridionally-confined "storm track", the gridded stirring field is windowed in the meridional direction with a Gaussian spatial mask centered at latitude θ_{stir} and having a half-width of 12°.

The model is integrated from pole-to-pole, but since the stirring is located in only one hemisphere, we restrict our analysis to that half of the globe. Each integration is spun-up for at least 500 days and then integrated an additional 12000 days for analysis. To aid the reader, we have defined a list of variables used regularly in our discussion in Table 1.

3. Eddy-length scale

Much of this work investigates the interaction between syntopic-scale eddies and the larger-scale mean flow. Eddy wave propagation and the resulting momentum fluxes are strongly dependent on the scale of the eddies themselves, and as such, we begin by determining the dependence of this scale on latitude. In addition, we demonstrate an optimal eddy-length scale for driving a strong westerly jet.

a. Change in eddy-length scale with latitude

When diagnosing Rossby-wave propagation on the sphere, it is useful to use Mercator coordinates so that the zonal wavenumber k of the wave along a ray is constant (Hoskins and Karoly 1981; Held 1983; Karoly 1983). In this case, the total wavenumber K^* is given by

$$K^* = \left(\frac{\beta_M}{\overline{u}_M - c_M} \right)^{1/2}, \tag{3}$$

where c_M is the phase speed of the wave in Mercator coordinates, $\overline{u}_M$ is the Mercator zonal velocity

$$\overline{u}_M = \overline{u}/cos\theta \tag{4}$$

and β_M is defined as

$$\beta_M = \frac{2\Omega\cos^2\theta}{a} - \frac{\cos\theta}{a^2}\frac{\partial}{\partial\theta}\left(\frac{1}{\cos\theta}\frac{\partial}{\partial\theta}\left(u\cos\theta\right)\right), \tag{5}$$

which is $\cos\theta$ times the meridional gradient of absolute vorticity on the sphere (β^*).

Hoskins and Karoly (1981) show that as a Rossby wave travels polewards, the meridional wavenumber l decreases and the latitude at which $k = K^*$ (or $l = 0$) acts as a turning latitude for the wave. Otherwise, the wave experiences a critical latitude when the phase speed equals the background zonal velocity. Another way to visualize this diagnostic is to rearrange (3) to obtain

$$K^* = \cos\theta\left(\frac{\beta^*}{\overline{u}-c}\right)^{1/2}, \tag{6}$$

in terms of spherical coordinates. In this case, it is clear that K^* is the usual Rossby-wave relation, with the factor of $\cos\theta$ accounting for the spherical effect of k decreasing with latitude.

We pose the following question: How does the Rossby-wave scale change as the eddy-driven jet is located closer to the pole? Intuition would suggest that as β decreases toward the pole, larger scale waves are needed to balance zonal advection with retrogression associated with β. To test whether the scaling predicted by (6) is valid, the barotropic model is stirred at various latitudes to test how the latitude of the jet influences the scale of the Rossby waves. The wavenumbers over which the model is stirred can effect the resulting eddy-scale, so, to remove any bias, we stir the model with *white noise*, constructed such that each wavenumber pair (l, m) is stirred identically, where l is now the total wavenumber of a spherical harmonic expansion of vorticity and m is the zonal wavenumber. We stir over wavenumbers $1 \leq l \leq 42$ and $m \geq 1$ and window the stirring field with a Gaussian mask at varying θ_{stir} latitudes. The strength of the stirring is normalized by ensuring that the time-averaged energy injection rate of the stirring $(-\overline{\psi \cdot \mathcal{S}})$ averaged over the hemisphere is constant across all integrations (Smith et al. 2002).

Fig. 1a shows the stirring total-wavenumber l spectra for three characteristic integrations and confirms that the stirring input is the same for each integration. The resulting vorticity-power spectra for the same integrations are displayed in Fig. 1b, where we have excluded the zonal-mean $(m = 0)$ component to focus on the eddy contribution. Although the stirring spectrum is similar in all integrations, the wavenumber of the peak of the vorticity-power spectrum $(\hat{l})$ shows a clear shift to smaller values as the jet is forced closer to the pole. To summarize this result, we define $\hat{l}$ from Fig. 1b by fitting a second-order polynomial about the peak of the spectrum and finding the peak wavenumber. Fig. 2a shows $\hat{l}$ plotted as solid circles against the latitude of the resulting eddy-driven jet θ_{edj} which is calculated by averaging the daily latitudes of the maximum zonal-mean zonal winds.

The question remains whether the increase in eddy scale with latitude is due simply to linear Rossby-wave scaling on a sphere. To investigate this question, we perform a series of quasilinear model integrations. The model setup is identical to the fully nonlinear case, except that the stirring power $\mathcal{S}^2$ is 0.01 times its value in the nonlinear runs and the zonal-mean vorticity tendency due to the eddies is multiplied by 100. Because the wave amplitudes remain small in these integrations, they behave linearly, and so if quasilinear theory is enough to explain the formation of the jet and the eddy scale, we expect the resulting zonal flow to be similar to that of the nonlinear integrations. The zonal-mean zonal winds for the fully nonlinear and quasilinear runs are plotted for two stirring latitudes in Fig. 3. While slight differences in the width and strength of the jet are evident, the quasilinear zonal wind is very similar to that of the fully nonlinear case, showing that linear wave propagation gives a reasonable approximation to the actual solution.

We plot $\hat{l}$ for the quasilinear integrations in Fig. 2a as open circles and see that even in the linear regime, the eddy scale increases ($\hat{l}$ decreases) as the jet moves poleward, suggesting that this change can be understood with linear arguments. The quasilinear eddy-length scale is always smaller than the nonlinear counterpart, and this may be partially due to the narrower jet in these integrations.

To determine whether linear theory (6) can predict this change in eddy scale with jet latitude, in Fig. 4 we plot the zonal wavenumber versus phase speed of the vorticity power spectrum at the latitude of the jet for two nonlinear integrations. The phase speed c is defined as the power-weighted phase speed over all wavenumbers (white cross in figure), and the resulting theoretical prediction given by (6) is plotted as black lines. It is clear from Fig. 4 that the actual spectra closely resemble that predicted by theory.

Fig. 4 alone does not answer the question as to how the Rossby-wave scale changes with jet latitude, as the spatial scale associated with zonal wavenumber k is a function of latitude itself. The total spectral wavenumber $\hat{l}$, however, represents a physical scale of the eddies independent of latitude. In this case, the prediction for $\hat{l}$ is $K^* \times (\cos\theta)^{-1}$ to convert from a zonal wavenumber to a physical spatial scale. This prediction is plotted as solid lines in Fig. 2a for both the nonlinear and quasilinear integrations and does a reasonable job predicting the eddy-length scale.

Work by Kidston et al. (2010) using 21st Century simulations suggests that the eddy-length scale will increase by 3%-7% as the climate warms and the jets shift polewards. To test whether jet latitude can explain this scale change, we follow Kidston et al. (2010) and define the eddy zonal wavenumber at each latitude as

$$\overline{k}(\theta) = \frac{\sum\limits_{k} k \times |\tilde{v}(k)|^2}{\sum\limits_{k} |\tilde{v}(k)|^2}, \tag{7}$$

where $\tilde{v}$ is the Fourier component of the 30-day highpass filtered meridional wind (see Kidston et al. (2010) for details). The zonal eddy length $\overline{\lambda}$ is defined as the mean of $2\pi a \cos\theta / \overline{k}(\theta)$ over the hemisphere.

The results are plotted in Fig. 2b and show that indeed, as previously seen using the total spectral wavenumber (Fig. 2a), the physical scale of the equilibrated Rossby waves increases as the mean jet is found at higher latitudes. In addition, we calculate a percentage change in eddy-length scale of about 5% due solely to a shift of the midlatitude jet from 46^{o}N to 52^{o}N. Although it appears to be the simplest explanation, further work is required to determine whether this barotropic-scale argument is the primary explanation for the behavior in more complex models.

b. *Importance of synoptic waves for driving a jet*

Fig. 1b demonstrates that even with white stirring, the equilibrium-eddy scale is skewed toward small wavenumbers. It is in fact these synoptic-scale Rossby waves that are responsible for the formation and maintenance of a strong zonal jet. To demonstrate the sensitivity of the resulting jet to eddy scale, the model is integrated for three different stirring configurations. The model is stirred with *white noise* ($1 \le l \le 42$), *synoptic-scale* ($4 \le l \le 10$), and *high-wavenumber* ($10 \le l \le 42$) stirring. In all three integrations, the zonal wavenumber m is confined to the same range as the total wavenumber l. As in previous experiments, a Gaussian mask with half-width 12° is applied to the stirring fields to mimic a localized storm track, and the stirring is centered at 45° N for all three integrations.

The stirring strength $\mathcal{A}$ for each run is defined such that the globally integrated energy injection rate ($-\overline{\psi \cdot \mathcal{S}}$) is constant across the integrations. Fig. 5a plots the prescribed stirring power versus total wavenumber for the three integrations. While we define the synoptic stirring experiment over wavenumbers 4 to 10, the resulting stirring spectrum exhibits power up to wavenumber 15. This apparent inconsistency is due to the Gaussian window which slightly alters the final stirring spectrum on the high-wavenumber edge. We have confirmed that the latitude of the window does not affect the stirring spectum, but rather the spectrum is most sensitive to the width of the window, which remains constant throughout this work.

The resulting vorticity power spectra and zonal winds are plotted in Fig. 5b,c for the three integrations. $\hat{l}$ is similar for both the white noise and synoptic stirring integrations, as may be expected when the jet scale and eddy scale co-evolve to a dynamical equilibrium. For white noise stirring, the zonal-mean jet forms at the latitude of stirring, with easterlies on both flanks, indicative of the presence of large-scale Rossby waves that are able to propagate and break to the north and south. The synoptically stirred jet has stronger winds that lie slightly poleward of the stirring, and the easterlies on the poleward flank of the jet are much weaker compared to the white noise wind profile. The reason for this is that only very large-scale waves are able to propagate and decelerate the flow near the pole (as described in Section 4), and unlike the white noise stirring, the synoptic stirring omits wavenumbers

1-3.

In the integration where only high wavenumbers are stirred, the vorticity spectrum peaks around 19, and the jet is weak and equatorward of the region of stirring. These features are due to the inability of the small-scale waves to propagate and break near the pole, and so, the equilibrium jet can only be sustained at a more equatorward latitude. The importance of synoptic scales can also be seen by the fact that synoptic stirring produces a stronger jet than white noise stirring, although the energy injection rate is identical for each. The difference lies in the forcing in the synoptic range, where the synoptic stirring has nearly twice the power at these scales.

SECTION SUMMARY

- Synoptic-scale Rossby waves ($4 \leq l \leq 10$) are essential to the formation and maintenance of the eddy-driven jet.
- As the mean jet is located closer to the pole, the eddy-length scales must increase because of the need to balance zonal advection with retrogression associated with the smaller value of β. Model results confirm that this scale is reasonably predicted by linear Rossby-wave theory.
- The predicted change in eddy-length scale due only to a poleward shift of the jet agrees with scale changes seen in GCM global warming simulations.

4. Changes in jet variability with latitude

We now investigate the interactions between the eddies and the mean flow as the latitude of the jet is varied. Previous studies have shown that the latitude of the jet influences the persistence of jet anomalies and that the leading mode of variability changes from a shift to a pulse as the mean jet is found closer to the pole (Barnes et al. 2010; Barnes and Hartmann 2010). In a barotropic model, changes in the variability of the jet are solely due to changes in the eddy-mean flow interaction, and so in this section we investigate the effect of latitude on jet variability and suggest a mechanism associated with changes in eddy-length scale and wave propagation.

We integrate (1) on the sphere and stir the model over total wavenumbers $8 \leq l \leq 12$, but require that $m \geq 4$ to ensure that we are not forcing at the scale of the zonal-mean flow itself. In Section 3 we showed that the formation of a jet is most dependent on these synoptic-scale wavenumbers, and we have confirmed that white noise forcing does not change the basic behavior of these integrations. To determine the dependence of jet variability on latitude, θ_{stir} is varied in 5^o increments between 35^oN and 65^oN giving rise to the formation of jets at varying latitudes. The stirring strength $\mathcal{A}$ is held at a constant value for all integrations to simulate eddies of a similar strength, but the results are similar if the energy injection rate is held constant instead.

We begin by plotting snapshots of the absolute vorticity field for the most poleward and equatorward θ_{stir} in Fig. 6. From these plots, it is clear that the model displays Rossby wavebreaking and the stretching of vorticity filaments reminiscent of the real atmosphere. Fig. 7a displays the resulting zonal-mean, zonal-wind profiles for the same integrations.

Defining the latitude of the jet, θ_{edj}, as the mean of the time series of daily latitudes of maximum zonal-mean zonal winds (Z_{lat}), Fig. 8a shows that in all cases θ_{edj} lies on or slightly poleward of θ_{stir}. The propensity for the jet to lie poleward of the stirring latitude is likely due to the $1/\beta$ relationship between $\overline{u}$ and the vorticity stirring source in the pseudomomentum budget, which causes eddies in the poleward half of the stirring region to more strongly force the jet.

Barnes et al. (2010) showed that as the mean jet is located nearer to the pole, the easterlies on the poleward flank vanish due to a lack of wavebreaking and associated deceleration of the winds there. Fig. 7a shows a similar result. We diagnose eddy propagation and wavebreaking using K^*, as defined previously in (6). According to linear theory, zonal wavenumber k turns when it reaches the latitude where $k = K^*$ and propagates toward larger values of K^*, breaking near its critical latitude, found where K^* is large (Hoskins and Karoly 1981; Held 1983).

We define the phase speed c in (6) as done in the previous section by calculating the vorticity-power-weighted phase speed at the latitude of the jet. The resulting K^* profiles are plotted in Fig. 7b and show that when $\theta_{stir} = 35^o$, the eddies break on both flanks of the jet, producing easterlies. However, when $\theta_{stir} = 65^o$ all wavenumbers encounter a turning latitude on the poleward edge of the jet, and thus waves only propagate and break on the equatorward flank. Profiles of K^* suggest that only the largest waves can propagate near the pole, and this result is consistent with the shift of the eddy-length scale to larger wavelengths as the stirring moves poleward, as seen in Section 3.

To further support the lack of equatorward momentum flux by the eddies when the jet is at high latitudes, we plot phase speed/latitude momentum flux spectra in Fig. 9. It is clear from these plots that for $\theta_{stir} = 35^o$, a small amount of equatorward eddy-momentum flux occurs on the poleward flank of the jet, but when the stirring is moved to 65^o, the eddies only transport momentum poleward.

The question remains, how does the variability of the jet change as θ_{edj} is located closer to the pole? Histograms of jet latitude Z_{lat} are plotted in Fig. 7c and show that jets closer to the pole move around less than those closer to the equator. To explore this change in jet variability with latitude, we define two more time series to describe the variability of the jet. Z_{speed} is the daily maximum zonal-mean zonal wind strength and captures the daily strengthening and weakening of the jet peak. In addition, we utilize Empirical Orthogonal Function (EOF) analysis to define the mode of variability that describes the largest variance of the zonal-mean zonal wind field and denote the associated principal component time series as Z_{eof1}.

Fig. 8b displays the percent of the total variance of the zonal-mean zonal wind field explained by each of the three time series $(Z_{lat}, Z_{speed}, Z_{eof1})$. The histograms in Fig. 7c suggest that the jet shifts less at higher latitudes, and indeed, Fig. 8b shows that Z_{lat} explains less of the total variance at high latitudes, and Z_{speed} explains more. The leading EOF captures the pattern that accounts for the highest percentage of the total variance, and we see that at low to mid latitudes, Z_{eof1} appears similar to Z_{lat}, but poleward of 55^oN, the leading mode of variability is described by the speed of the jet, not its shift. Fig. 8c displays the magnitude of the EOF jet shift, defined as the meridional distance between the latitude of the mean jet and the latitude of the jet associated with 1 standard deviation of Z_{eof1}. As the jet moves poleward, the leading mode of variability is associated less with meridional movement and more with the strength of the jet.

We can understand these changes in variability with latitude by considering the influence of the pole on eddy propagation and wavebreaking. The strength of the positive feedback between the zonal-flow and the eddies depends upon the ability of the mean-flow to influence the eddies by setting the critical latitudes, and in turn, the ability of the eddies to influence the jet by decelerating the flow where they break and thence flux momentum back into the jet core. When the jet is far from the pole, random fluctuations of the eddy forcing shift the jet, which shifts the critical latitudes, which in the end, shifts the distribution of momentum flux such that the jet can be maintained in its new position. When the jet is near the pole, random fluctuations of the eddy forcing may still move the eddy-driven jet poleward, but the small value of β^* due to the small value of β in (6) creates a turning latitude and thus the jet is unable to set a new poleward critical latitude. Since the critical latitudes set the eddy-momentum flux distribution, the eddy-driven jet will not be sustained there.

In the real atmosphere, the dominant variability of the midlatitude jet involves both a shift and a pulse. The leading mode of variability of the North Atlantic jet is termed the North Atlantic Oscillation (NAO) and describes oscillations between an equatorward eddy-driven jet and a poleward, strengthened jet (Hurrell et al. 2003). Woollings et al. (2010) argue that characterizing the full-range of variability of the North Atlantic jet requires descriptions of both the strength and the latitudinal position of the jet. Both of these results are consistent with our findings that the variability of a jet in midlatitudes experiences a mix of shifting and pulsing variability due to its proximity to the pole.

SECTION SUMMARY

As the eddy-driven jet moves poleward:

- the leading mode of variability of the eddy-driven jet changes from a meridional shift to a pulse of the jet.
- the feedback between the zonal-flow and the eddies is reduced due to the inability of the eddies to propagate and break at high latitudes.

5. Dynamics of a pulsing jet

Previous studies have demonstrated that a pulse of the eddy-driven jet is less persistent than a meridional shift of the jet due to the presence of a positive eddy feedback during the shifting mode and no such feedback during a pulsing mode (Lorenz and Hartmann 2001; Eichelberger and Hartmann 2007). Here, we suggest a mechanism for the presence of a negative feedback during pulsing mode events, which forces the jet back to its equilibrium state and accounts for the lack of persistence.

Fig. 10a shows composites of the zonal wind of the $\theta_{stir} = 35^{o}$N integration for the top and bottom 10% of Z_{speed}. The profiles of K^* associated with these wind fields are plotted in Fig. 10b for phase speeds calculated as before and this figure shows that ultimately, K^* decreases at the jet core for strong winds, implying that only the largest Rossby waves can propagate and break away from the jet within the stronger zonal flow. We plot the momentum flux convergence two days after the strengthening event in Fig. 10c to demonstrate that the eddy-momentum forcing is weaker immediately following the pulse. This reduction in momentum flux convergence after the initial pulse acts as a negative feedback on the stronger jet, and the jet subsequently weakens back to its original strength. A similar story is seen when the jet weakens from its equilibrium value. In this case, K^* suggests that more waves are able to propagate away and break, and thus more momentum converges into the jet region. Once again, this is a negative feedback on a weakened jet, and the jet profile returns to its equilibrium value.

The linear diagnostic K^* suggests that after a strengthening of the jet, the anomalous eddy propagation is into the jet and the anomalous eddy-momentum flux across the jet flanks is *out of the jet*, acting to weaken the jet. Likewise, after the weakening of the jet, the anomalous eddy propagation is out of the jet, resulting in more eddy-momentum being fluxed *into the jet core*. To confirm that this is the case, we calculate lagged-correlations of Z_{speed} and the anomalous eddy-momentum flux across latitude circles 10^o equatorward and poleward of the mean jet. The results for the $\theta_{stir} = 35^o$ integration are plotted in Fig. 11, where positive correlations imply anomalous eddy momentum fluxes *into the jet* (eddy propagation away from the jet) and positive lags imply that the jet leads the forcing. Focusing on the equatorward latitude circle first, there is an anomalous positive flux of momentum into the jet a day or two before a pulsing event, which is clear evidence of the eddies strengthening the jet. Lorenz and Hartmann (2001) showed that a positive eddy-mean flow feedback manifests itself as positive correlations at positive lags. However, Fig. 11 shows that no feedback is present, and the eddies extract momentum from the jet at positive lags, returning the jet to its mean state. This is consistent with Fig. 10b,c, which suggests that the stronger jet inhibits wave propagation away from the jet, reducing the amount of momentum fluxed into its core.

We can also compare the eddies on each flank of the jet, and focusing now on the poleward latitude circle of Fig. 11, one might be surprised to see that it is not identical to that of the equatorward curve, but rather, the anomalous momentum flux across this poleward latitude circle is *out of the jet core* at all lags. This implies that a strengthening jet has anomalous equatorward eddy propagation across its poleward flank, both before and after the event. The reason for this is due to the linear Rossby-wave-propagation arguments of the previous sections, whereby the pole inhibits Rossby-wave propagation. The only way for the poleward eddies to strengthen the jet is for the waves to propagate anomalously equatorward, not poleward. Fig. 11 demonstrates that even fewer waves propagate poleward during a strengthening event, a conclusion that was also drawn from Fig. 10b, where K^* suggests that fewer waves are able to propagate toward the pole when the jet strengthens and β^* increases.

As the jet shifts poleward, the dominant variability changes from a shift to a pulse, and the eddies act as a negative feedback on the strengthening and weakening jet. Consistent with this mechanism, recent work has shown that the leading mode of variability becomes less persistent as the jet is found at higher latitudes, both in a barotropic model and in general circulation models (Barnes et al. 2010; Barnes and Hartmann 2010).

It is possible that barotropic instability on the poleward jet flank may also bring about the decay of a pulsing jet. However, for the wind profiles simulated by this model, only the lowest zonal wavenumbers are unstable and the growth rates are very slow with e-folding times on the order of weeks. In addition, eddy momentum fluxes by the unforced wavenumbers 1-3 contribute little to the total momentum flux into and out of the jet during pulsing events (not shown), implying that normal mode growth on the polar flank of the jet cannot explain the decay of the pulsing mode in the model.

SECTION SUMMARY

- When the jet strengthens, $\overline{u}$ and β^* increase, resulting in a modified K^* profile.
- Plots of K^* suggest that the eddies are less likely to propagate away from the jet core during a strengthening event, which acts as a negative feedback on the pulsing jet.
- For jets close to the pole, the eddies on the poleward flank are less able to propagate poleward, and thus the momentum flux toward the jet center is reduced. In this situation, the eddies on the equatorward side dominate the driving, and it is the convergence of poleward momentum flux that drives the pulsing of the jet.

6. Influence of the subtropical jet on eddy-driven jet latitude and variability

Thus far, we have looked poleward to determine the constraints on jet variability and the eddy-mean flow interaction set by the dependence of β on latitude. In this section, we look equatorward to study the influence of a strong subtropical jet on the location and variability of the eddy-driven jet. We demonstrate that the subtropical winds can influence the location of the critical latitudes through modification of u in (6), thus influencing the latitude of the eddy-driven jet and breaking the positive feedback loop between the eddies and the eddy-driven jet, thereby changing the eddy-driven jet's variability.

To analyze the influence of the subtropical jet on eddy-mean flow interactions, the latitude of the subtropical jet θ_{sub} is held fixed at 30°N. The stirring is varied every 5° from 35°N to 65°N with stirring over total wavenumbers $8 \leq l \leq 12$ and $m \geq 4$ and constant stirring strength $\mathcal{A}$.

The subtropical jet is modeled as a Gaussian in zonal wind

$$u_{sub}(\theta) = \mathcal{U} \exp\left(\frac{-(\theta - \theta_{sub})^2}{2\sigma_{sub}^2}\right), \tag{8}$$

where $\sigma_{sub} = 6^{\mathrm{o}}$ and $\mathcal{U}$ is the speed of the subtropical jet, which is set to 20 m/s, and we have verified that the subtropical jet is barotropically stable with these parameters. The vorticity equation from (1) is integrated forward with the stirring ($\mathcal{S}$) and relaxed back to the subtropical jet profile ζ_{sub} derived from (8)

$$\frac{\partial \zeta}{\partial t} + \frac{u}{a\cos\theta}\frac{\partial \zeta}{\partial \lambda} + \frac{v}{a}\frac{\partial \zeta}{\partial \theta} + v\beta = \mathcal{S} - r(\zeta - \zeta_{sub}) - \kappa\nabla^4(\zeta - \zeta_{sub}), \tag{9}$$

where values for r and κ are the same as in Section 4.

a. Eddy-driven jet variability in the presence of a subtropical jet

Eichelberger and Hartmann (2007) showed that the leading mode of variability of the eddy-driven jet changes from a shift to a pulse in the presence of a strong subtropical jet and they suggest that the subtropical jet acts as a waveguide, allowing the eddies to propagate downstream, inhibiting the positive feedback between the eddies and the background flow. Our work suggests that similar relationships are found in barotropic simulations.

Fig. 12a–d displays zonal-mean zonal wind profiles for different latitudes of eddy stirring. The solid curve denotes the total zonal-mean zonal-wind, while the dashed line denotes the part associated with the fixed subtropical jet (8). Because the zonal wind would exactly equal the specified subtropical jet if eddies were not present, we subtract the subtropical profile from the total zonal-wind profile to obtain the zonal wind deviation associated with eddies, or the "eddy-driven jet". Plotted alongside the zonal wind profiles in Fig. 12a–d are histograms of the eddy-driven jet latitude Z_{lat}, defined as the daily latitude of maximum zonal-mean eddy-driven zonal wind. When $\theta_{stir} = 35^{\circ}$N, the subtropical and eddy-driven jets merge and become one strong jet, similar to that seen in the North and South Pacific during their respective winter seasons (Eichelberger and Hartmann 2007; Nakamura and Shimpo 2004). When the jets are merged in the barotropic model, the meridional movement of the eddy-driven jet is restricted, as indicated by the narrowness of the histogram. As the stirring moves poleward, the eddy-driven jet shifts more freely, with the jet latitude histogram skewed toward high latitudes.

Since the critical latitudes depend on the difference between the eddy phase speeds and the background flow u, the presence of a strong subtropical jet has the potential to greatly influence the location of eddy wavebreaking, and thus the location of the eddy-driven jet. Fig. 13a shows the eddy-driven jet latitude versus stirring latitude. As the stirring moves away from the subtropical jet, the latitude of the eddy-driven jet varies more slowly, such that the stirring lies poleward of the mean jet at $\theta_{stir} = 50^{\circ}$N. To understand this result, we use the reasoning in Section 4 and diagnose the locations of eddy wavebreaking.

Fig. 12e–h shows profiles of K^* for the four integrations. As the eddy stirring moves polewards, the equatorward critical latitude (maximum of K^*) remains stationary because it is set by the stationary subtropical winds. Even though the stirring moves poleward, the propagation environment for the eddies does not, and the eddy-driven jet does not move with the stirring, resulting in an eddy-driven jet equatorward of the stirring latitude. This can also be seen in Fig. 12a–d, where the most frequent latitude of the eddy-driven jet moves by only 4^o even though the stirring moves from 35^o to 50^oN. Interestingly, Lee and Kim (2003) used an idealized model to demonstrate that the most favorable region for baroclinic wave growth and latitude of the eddy-driven jet is approximately 20^o-30^o poleward of a modest subtropical jet. Results presented here suggest a similar barotropic relationship, such that the eddy-driven jet is likely to be found 15^o poleward of a strong subtropical jet due purely to the latitudes of eddy wavebreaking set by the background flow.

Fig. 12a–d suggests that when the eddy-driven and subtropical jets are merged, the meridional shifting of the eddy-driven jet is suppressed, and as the stirring is moved poleward, the meridional variability of the eddy-driven jet increases. To show this more clearly, we follow Section 4 and define Z_{speed} as the daily maximum zonal-mean zonal wind strength, and Z_{eof1} as the leading principal component of the zonal-mean zonal winds. Fig. 13b shows the percent of the total zonal-mean zonal wind variance explained by Z_{eof1}, Z_{lat} and Z_{speed}. When the stirring is at 35^oN, the pulsing of the jet explains more variance than the shifting, reminiscent of the variability of a jet near the pole. As the stirring moves away from the subtropical jet, the meridional shifting of the jet describes more of the variance. To display the type of variability associated with the leading EOF, Fig. 13c shows the shift of the eddy-driven jet associated with 1 standard deviation of Z_{eof1}. When the eddy-driven jet is merged with the subtropical jet, the leading mode of variability is associated with a small shift of 1^o of the jet. As the eddy-driven jet moves away from the subtropical jet, the leading mode of variability becomes associated with a stronger shift of the zonal winds, consistent with what was shown in Fig. 13b. These results are similar to what Eichelberger and Hartmann (2007) found over the Pacific Ocean in observations, where the presence of a strong subtropical jet causes the variability of the eddy-driven jet to change from a shift to a pulse of the zonal-mean zonal winds.

The shifting variability of the eddy-driven jet is inhibited by the subtropical winds because when the subtropical jet sets the critical latitudes, the positive feedback chain between the eddies and the eddy-driven jet is broken: the eddies continually break and thus reinforce the eddy-driven jet, but the eddy-driven jet does not set the equatorward breaking latitude since the winds are too weak and are dominated by the strong subtropical winds. In this case, the easterly eddy accelerations remain focused in the center of the subtropical jet, and so, the distribution of momentum flux convergence (jet forcing) is set by the stationary subtropical jet. As the stirring moves poleward, the eddy-driven jet slowly breaks away from the subtropical winds and begins to set its own critical latitudes, allowing the eddy-driven jet to move more freely.

b. Bimodal eddy-driven jet latitude

When the eddy stirring moves poleward of 50°N, the distribution of the latitude of the eddy-driven jet becomes more complex. Fig. 14a–c shows the jet latitude histograms along with the resulting zonal wind profiles for three such integrations. Unlike the distributions plotted in Fig. 12a–d, the eddy-driven jet latitudes become bimodal, with a clear preference to lie either on the flank of the subtropical jet, or farther poleward, at the latitude of the eddy-stirring.

Fig. 14d–f shows the eddy-driven zonal winds composited on days when the jet is poleward or equatorward of 54°N. As the stirring moves poleward from 55°N to 65°N, the latitude of the equatorward eddy-driven jet stays fixed at 46°N, indicating that this mode is still slave to the subtropical jet and its stationary critical latitude. The poleward eddy-driven jet moves with the eddy-stirring, which suggests that the jet is free to set its own critical latitudes, although the influence of the pole will restrict its meridional shifting as discussed in Section 4.

Fig. 14g–i displays profiles of K^* for days when the jet is poleward and equatorward of 54°N. The profiles are calculated using the vorticity-power weighted phase speed c at the latitude of the eddy-driven jet, and the black dots denote the position of the eddy-driven jet. Since the K^* profiles for all three integrations are similar, we will focus on the profiles for $\theta_{stir} = 65^{\circ}$N. When the jet is equatorward, the wavebreaking diagnostic suggests that waves starting at the center of the jet will propagate both poleward and equatorward toward large values of K^*. At these critical latitudes, the waves will break and produce an easterly acceleration of the winds, consistent with Fig. 14d–f. In this jet configuration, the equatorward critical latitude is set by the subtropical winds, and thus does not vary. When the eddy-driven jet is poleward, the profile of K^* is nearly identical to that of the $\theta_{stir} = 65^{\circ}$N with no subtropical jet present (see Fig. 7b). Waves propagate toward large values of K^*, and so waves starting at the center of the jet (65°N) will propagate equatorward only and break where K^*has a local maximum (50°N). In this instance, the poleward displaced jet is no longer as influenced by the subtropical critical latitudes.

Note that since the subtropical critical latitudes do not change, some eddies will always break there, causing a constant (albeit weak) region of westerlies at 45°N even when the eddy-driven jet is in its poleward mode (Fig. 14f).

Trimodal behavior of the eddy-driven jet was recently documented by Woollings et al. (2010) in the North Atlantic during winter (DJF), but not in the other seasons. During the winter months, the North Atlantic subtropical jet is strongest, and our results suggest that the presence of a strong subtropical jet could be enough to produce bimodal behavior of the latitude of the eddy-driven jet. Future work will explore whether this barotropic interaction between the subtropical and eddy-driven jet is enough to at least partially explain the preferred eddy-driven jet latitudes in the observations.

One might argue that the influence of the subtropical winds on the eddy-driven jet may be due to an change in the source of the eddies, rather than their dissipation. We have diagnosed terms in the pseudomomentum budget (see Vallis et al. (2004) for a discussion) for both fully nonlinear and quasilinear integrations and have found that changes in the latitude of the eddy-driven jet are largely associated with changes in the dissipation and not changes in the source of pseudomomentum. This implies that it is the modulation of the eddy wavebreaking, and not the eddy source, that provides the mechanism by which the subtropical and eddy-driven jets interact in this model.

SECTION SUMMARY

As the eddy-driven jet moves away from a fixed subtropical jet:

- the leading mode of variability of the eddy-driven jet describes less of a pulse and more of a meridional shift of the eddy-driven jet.
- the eddy-driven jet latitude becomes bimodal, representative of a free eddy-driven jet that sets its own critical latitudes and an eddy-driven jet that is wedged between its

own poleward critical line and the subtropical jet.

7. Discussion & Conclusions

The structure and variability of eddy-driven jets is strongly controlled by the location of critical latitudes and eddy wavebreaking. In high latitudes, the effects of β on Rossby wave propagation on the poleward side of the jet produce changes in the eddy-mean flow interaction, causing the leading mode of variability to change from a shift to a pulse of the jet. The presence of a strong subtropical jet near the equatorward edge of an eddy-driven jet reduces the eddy-driven jet variability by fixing the regions of wavebreaking. As the source of eddies moves away from the subtropical winds, the latitude of the eddy-driven jet becomes bimodal, with one regime describing a free eddy-driven jet and the other regime describing an eddy-driven jet influenced by the subtropical jet.

This work identifies a robust increase in eddy-length scale as the eddy-driven jet is located at higher latitudes in a nonlinear barotropic model, which highlights that the latitude of the eddy-driven jet and the characteristic eddy scale are inextricably linked. We find that in both the fully nonlinear and quasilinear integrations, the eddy length can be predicted by linear Rossby-wave theory, which predicts an increase in eddy-length scale of about 5% for a midlatitude jet shifting poleward from 46°N to 52°N. This percent increase agrees well with what is seen in global warming simulations (Kidston et al. 2010), suggesting that the eddy scale increase in these complex GCMs may be a simple consequence of barotropic dynamics.

While this work analyzed an idealized barotropic model, the question "how might the pattern of atmospheric variability change with a poleward shift of the jet?" is applicable to the real atmosphere. This work suggests that the “annular modes” will transition from a shift to a pulse of the zonal-mean zonal winds as the eddy-driven jet moves poleward with climate change. Additional analyses of more complex models and observations are required to determine whether the barotropic mechanisms described here are the most parsimonious explanation for the observed and modeled behaviors of eddy-driven jets.

Acknowledgments.

We wish to thank Peter Rhines, Ming Cai, Isaac Held, Geoff Vallis and two anonymous reviewers for their insightful and clarifying comments, which greatly improved this manuscript. This work supported by the Climate Dynamics Program of the National Science Foundation under grant AGS 0960497.

REFERENCES

Barnes, E. A. and D. L. Hartmann, 2010: Testing a theory for the effect of latitude on the persistence of eddy driven jets using the CMIP3 simulations. *Geophys. Res. Lett.*, **37**, L15 801, doi:10.1029/2010GL044144.

Barnes, E. A., D. L. Hartmann, D. M. W. Frierson, and J. Kidston, 2010: The effect of latitude on the persistence of eddy-driven jets. *Geophys. Res. Lett.*, **37**, L11 804, doi: 10.1029/2010GL043199.

Eichelberger, S. J. and D. L. Hartmann, 2007: Zonal jet structure and the leading mode of variability. *J. Climate*, **20**, 5149–5163, doi:10.1175/JCLI4279.1.

Held, I. M., 1983: Stationary and quasi-stationary eddies in the extratropical troposphere: Theory. *Large-scale dynamical processes in the atmosphere*, B. J. Hoskins and R. P. Pearce, Eds., Academic Press, London, 127–168.

Hoskins, B. J. and D. J. Karoly, 1981: The steady linear response of a spherical atmosphere to thermal and orographic forcing. *J. Atmos. Sci.*, **38**, 1179–1196.

Hurrell, J. W., Y. Kushnir, G. Ottersen, and M. Visbeck, 2003: An overview of the North Atlantic Oscillation. *The North Atlantic Oscillation: Climatic Significance and Environmental Impact*, Amer. Geophys. Union, No. 134 in Geophysical Monotraph.

Karoly, D. J., 1983: Rossby wave propagation in a barotropic atmosphere. *Dyn. Atmos. Oceans*, **7**, 111–125.

Kidston, J., S. M. Dean, J. A. Renwick, and G. K. Vallis, 2010: A robust increase in the eddy length scale in the simulation of future climates. *Geophys. Res. Lett.*, **37**, doi: 10.1029/2009GL041615.

Kidston, J. and E. Gerber, 2010: Intermodel variability of the poleward shift of the austral jet stream in the CMIP3 integrations linked to biases in the 20th centery climatology. *Geophys. Res. Lett.*, **37**, L09 708, doi:10.1029/2010GL042873.

Lee, S. and H.-K. Kim, 2003: The dynamical relationship between subtropical and eddy-driven jets. *J. Atmos. Sci.*, **60**, 1490–1503.

Lorenz, D. J. and D. L. Hartmann, 2001: Eddy-zonal flow feedback in the Southern Hemisphere. *J. Atmos. Sci.*, **58**, 3312–3327.

Nakamura, H. and A. Shimpo, 2004: Seasonal variations in the Southern Hemisphere storm tracks and jet streams as revealed in a reanalysis dataset. *J. Climate*, **17**, 1828–1844.

Smith, K., G. Boccaletti, C. Henning, I. Marinov, C. Tam, I. Held, and G. Vallis, 2002: Turbulent diffusion in the geostrophic inverse cascade. *J. Fluid Mech.*, **469**, 13–48.

Vallis, G. K., E. P. Gerber, P. J. Kushner, and B. A. Cash, 2004: A mechanism and simple dynamical model of the North Atlantic Oscillation and annular modes. *J. Atmos. Sci.*, **61**, 264–280.

Woollings, T., A. Hannachi, and B. Hoskins, 2010: Variability of the North Atlantic eddy-driven jet stream. *Quart. J. Roy. Meteor. Soc.*, **136**, 856–868, doi:10.1002/qj.625.

List of Tables

Table 1: definitions

θ_{sub}	latitude of the center of the subtropical jet
θ_{edj}	latitude of the resulting eddy-driven jet
θ_{stir}	latitude of the center of the stirring
Z_{lat}	daily time series of the latitude of the eddy-driven jet
Z_{speed}	daily time series of the maximum speed of the eddy-driven jet
Z_{eof1}	daily time series of the leading EOF of zonal-mean zonal wind
$\hat{l}$	peak total wavenumber of the vorticity spectrum
$\overline{\lambda}$	zonal eddy-length scale

List of Figures

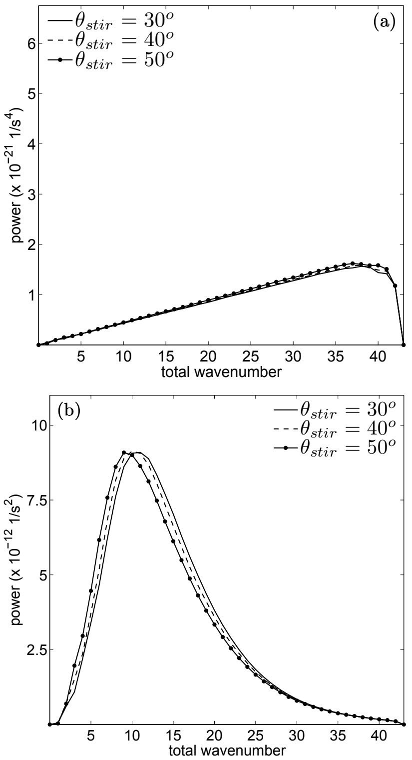

Figure 1: (a) Vorticity stirring ($\mathcal{S}$) power versus total wavenumber l after windowing the field. (b) Vorticity power versus total wavenumber. In all experiments, the zonal wavenumber m is restricted to the same range as l, but we plot only the eddy contributions ($m \neq 0$).

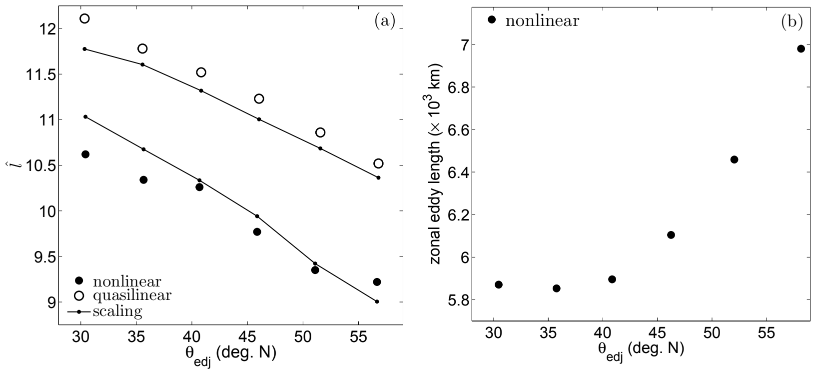

Figure 2: (a) The total wavenumber at which the eddy vorticity spectrum is maximum ($\hat{l}$) for both nonlinear and quasilinear integrations. The wavenumbers predicted by theory are denoted by the black lines (see text for details). (b) Zonal eddy length scale ($\overline{\lambda}$) versus eddy-driven jet latitude for the nonlinear integrations.

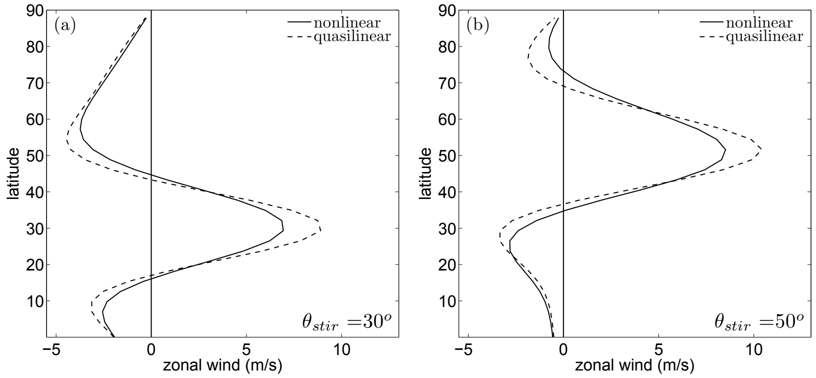

Figure 3: Zonal-mean zonal winds for the nonlinear and quasilinear integrations for two different stirring latitudes.

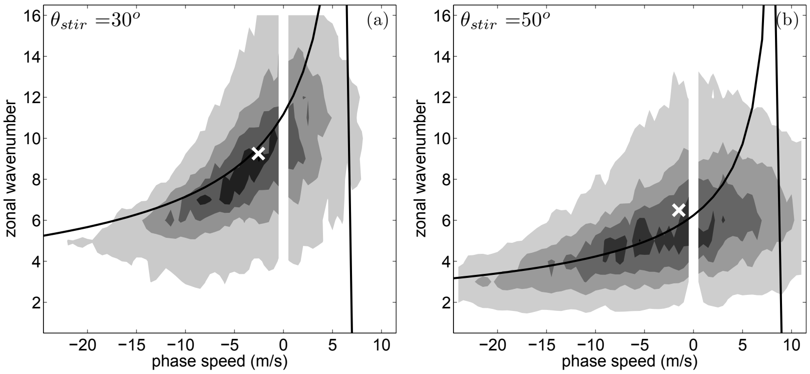

Figure 4: (a,b) Zonal wavenumber, phase-speed vorticity-power spectrum. Black lines denote the theoretical prediction (6) and the white cross denotes the power-weighted-average wavenumber and phase speed. Contours for $\theta_{stir} = 30^{\rm o}$ ($\theta_{stir} = 50^{\rm o}$) are shaded every 3.5 (5.0) $\times 10^{-13}$ sec^{-2}.

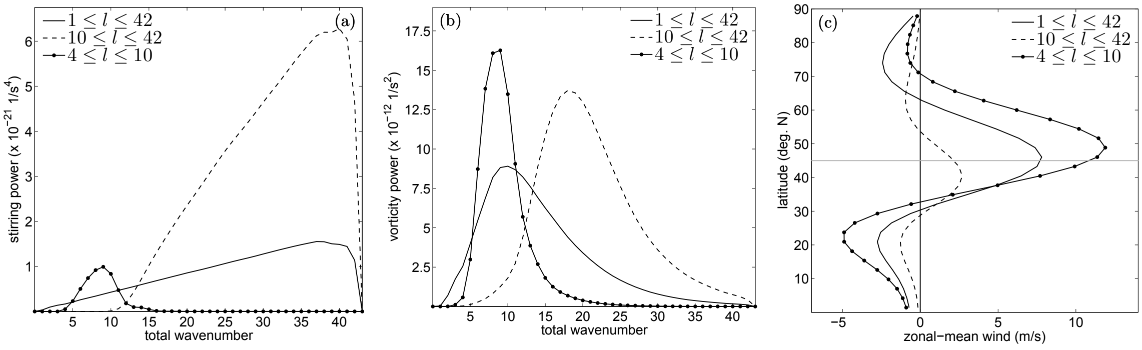

Figure 5: (a) Vorticity stirring ($\mathcal{S}$) power versus total wavenumber l after windowing the field. (b) Resulting vorticity power versus total wavenumber l. In all three experiments, the zonal wavenumber m is restricted to the same range as l, but we plot only the contributions from waves with $m \neq 0$. (c) Zonal-mean zonal-wind profiles.

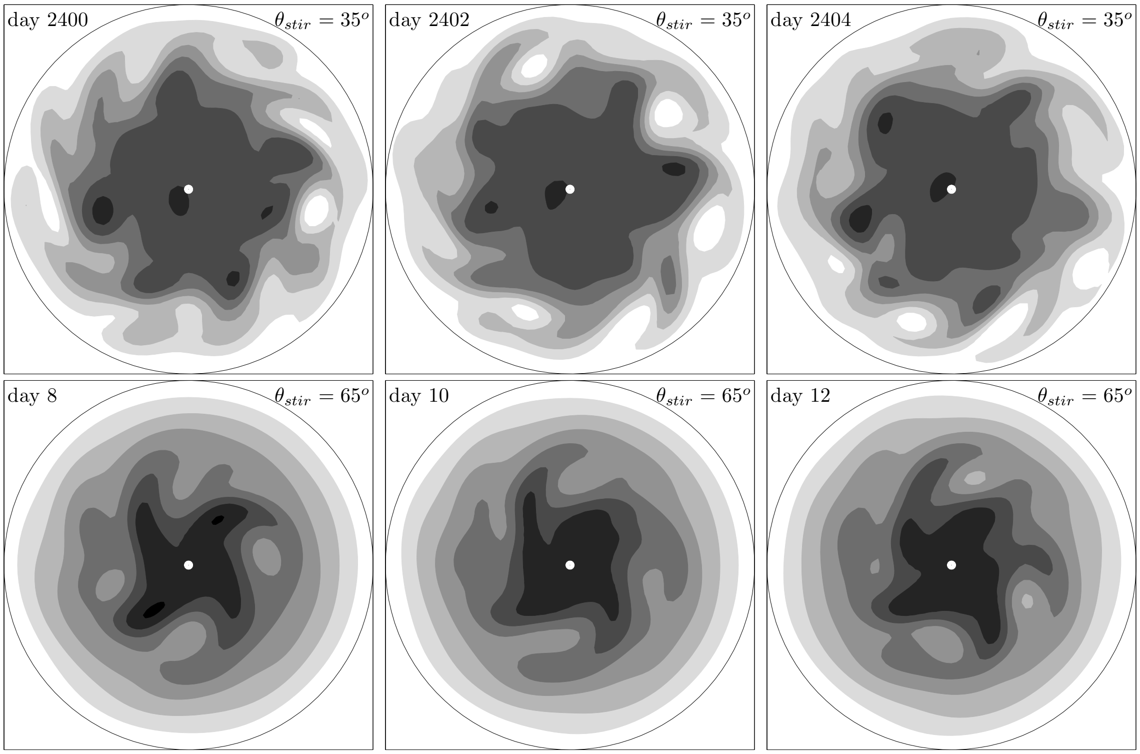

Figure 6: Absolute vorticity fields for integrations with $\theta_{stir} = 35^{\text{o}}$ and $\theta_{stir} = 65^{\text{o}}$. The shading is contoured every 2.5×10^{-5} sec^{-1} where darker colors denote larger values.

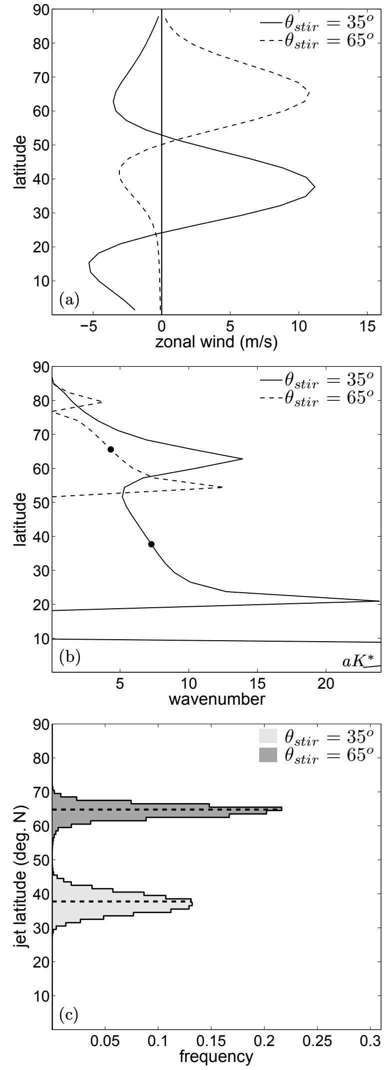

Figure 7: (a) Average zonal-mean zonal wind profiles for integrations where the stirring latitude is varied. (b) K^* times the radius of the earth a for the vorticity power-weighted phase speed c at the latitude of the jet. The filled circle denotes the latitude of the eddy driven jet (θ_{edj}). (c) Histograms of daily eddy-driven jet latitude (Z_{lat}) frequency for different θ_{stir}. Mean jet latitudes are plotted as thick dashed horizontal lines.

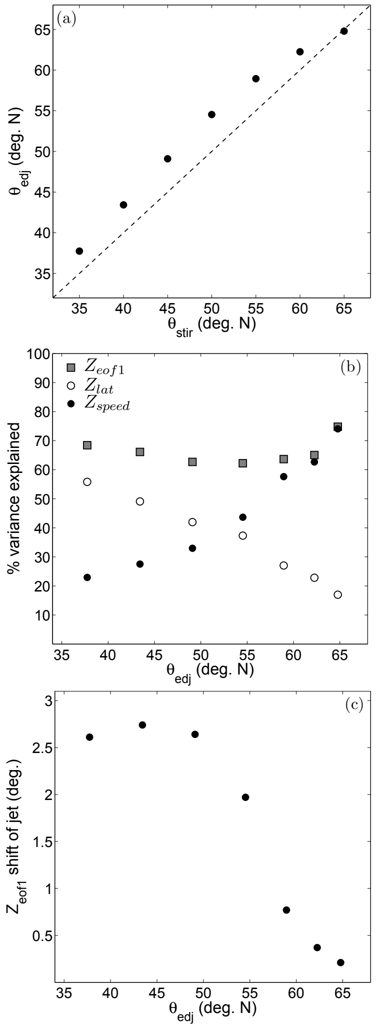

Figure 8: (a) The latitude of the eddy-driven jet (θ_{edj}) versus the latitude of eddy stirring (θ_{stir}). The dashed line denotes the one-to-one line. (b) The percent of the total variance of the zonal-mean zonal wind explained by Z_{eof1}, Z_{lat} and Z_{speed}. (c) The shift of the eddy-driven jet associated with one standard deviation of the leading EOF (Z_{eof1}) versus θ_{edj} for integrations with varying stirring latitudes.

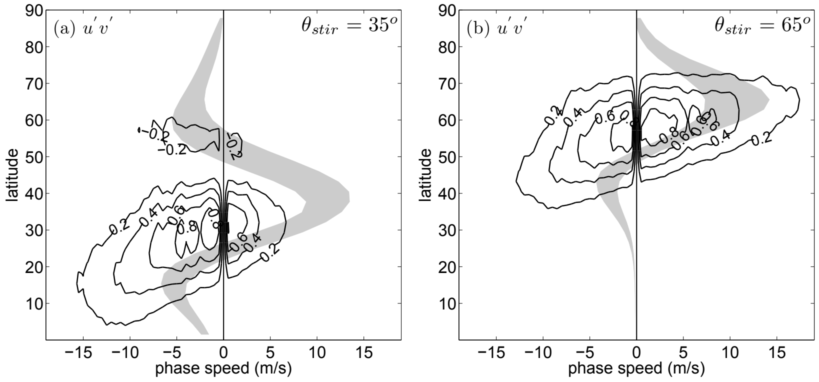

Figure 9: Contours of transient eddy momentum flux versus latitude and phase speed for integrations with $\theta_{stir} = 35^{\circ}$ and $\theta_{stir} = 65^{\circ}$. Shading denotes plus and minus one standard deviation of the daily zonal-mean zonal winds.

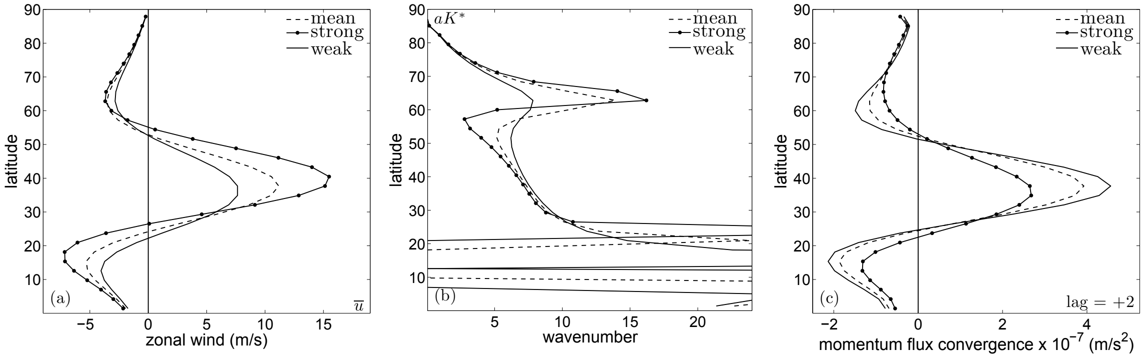

Figure 10: (a) Zonal-mean zonal wind profiles for the mean and extremely strong and weak jet strength days. (b) K^* times the radius of the earth a for the vorticity power-weighted phase speed c at the latitude of the jet. (c) Profiles of the eddy momentum-flux convergence for the mean and two days after extremely strong and weak jet strength days. Plots are of the $\theta_{stir} = 35^{o}$N integration.

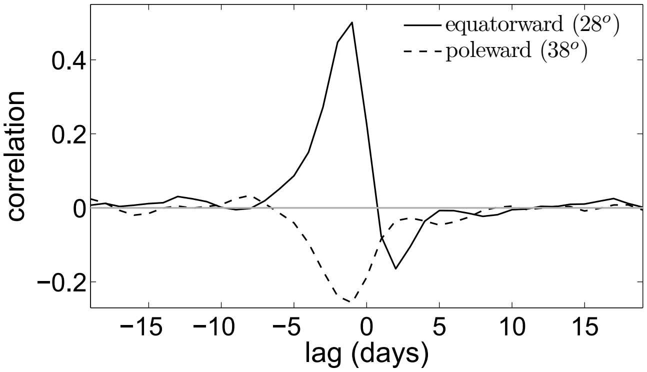

Figure 11: Lagged-correlation over all pulsing days of Z_{speed} and the anomalous eddy momentum flux *into* the jet core at latitudes 10^{o} equatorward and poleward of the time-mean jet for $\theta_{stir} = 35^{\mathrm{o}}$.

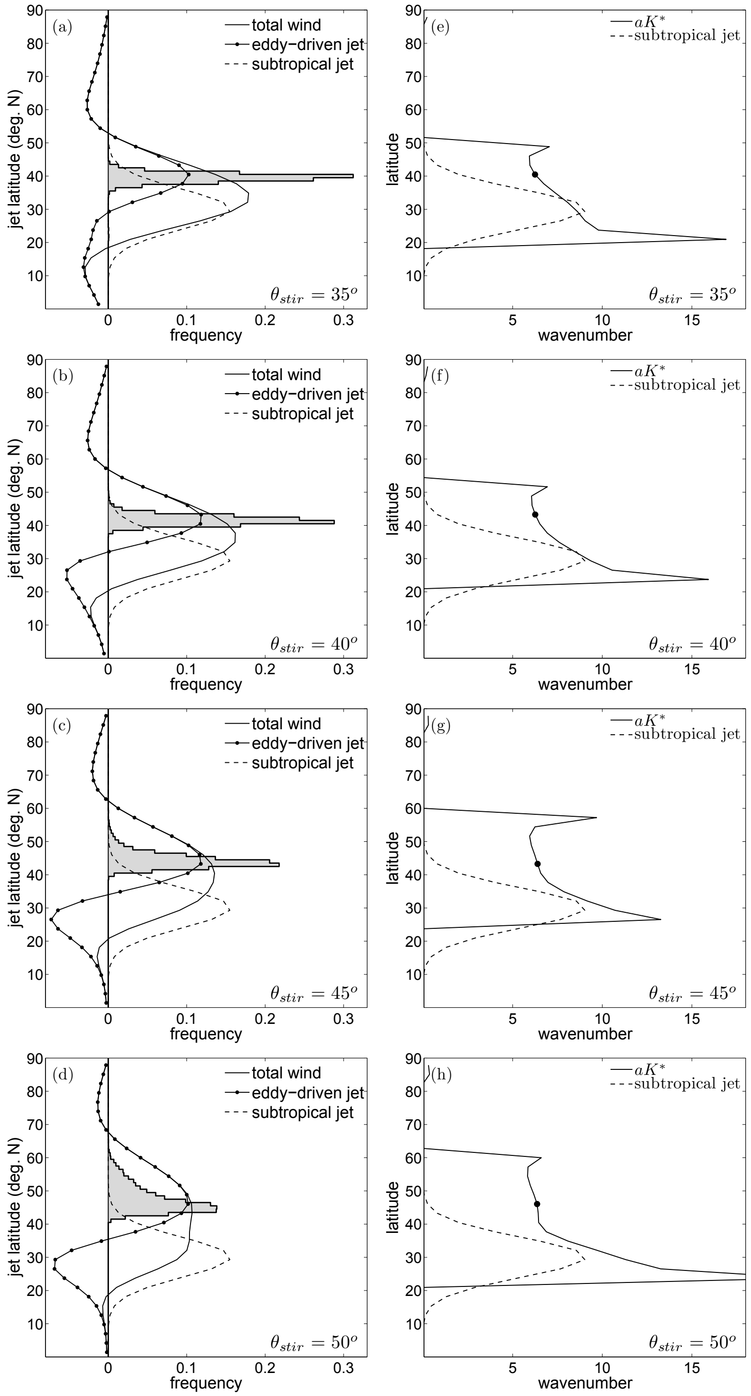

Figure 12: (a–d) Histograms of daily eddy-driven jet latitude (Z_{lat}) frequency for different stirring latitudes. The zonal-mean wind profiles of the total zonal wind, fixed subtropical jet, and resulting zonal eddy-driven jet are plotted in scaled units (20 m/s $\sim$ 0.15). (e–h) K^* times the radius of the earth for the vorticity power-weighted phase speed c at the latitude of the jet. The filled circle denotes the latitude of the eddy driven jet.

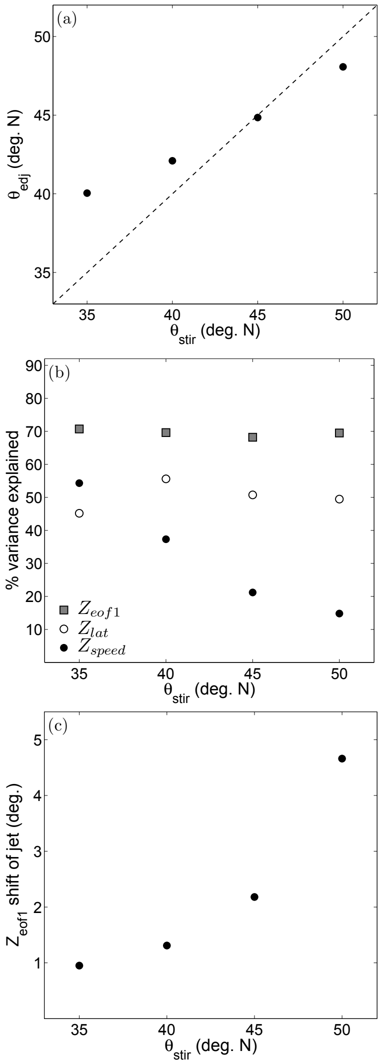

Figure 13: (a) The latitude of the eddy-driven jet (θ_{edj}) versus the latitude of eddy stirring (θ_{stir}). The dashed line denotes the one-to-one line. (b) The percent of the total variance of the zonal-mean zonal wind explained by Z_{eof1}, Z_{lat} and Z_{speed}. (c) The shift of the eddy-driven jet associated with one standard deviation of the leading EOF (Z_{eof1}) versus θ_{edj}. A subtropical jet is fixed at $\theta_{sub} = 30^{o}$N with a strength of 20 m/s for all integrations.

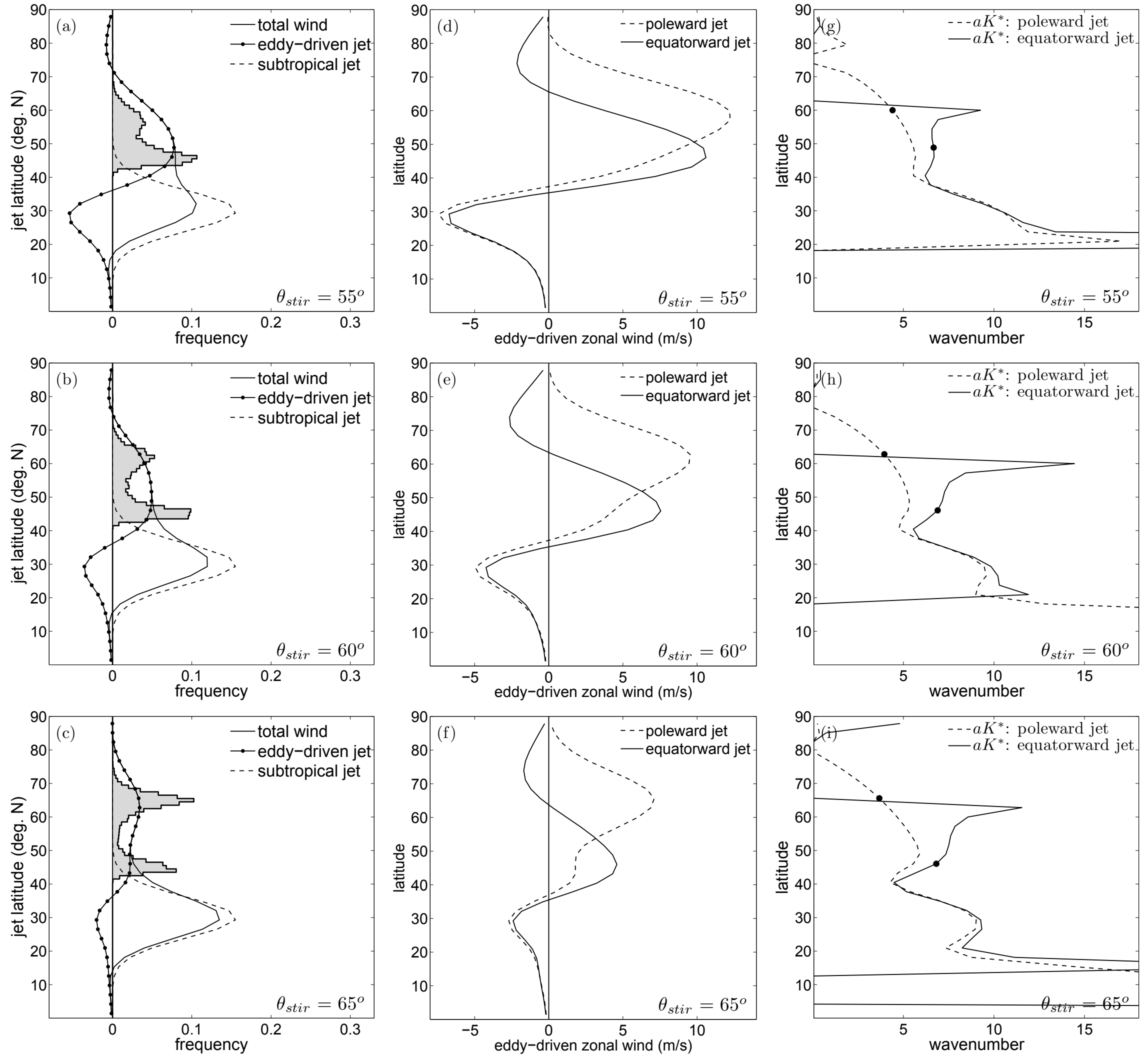

Figure 14: (a–c) Histograms of daily eddy-driven jet latitude (Z_{lat}) frequency for different stirring latitudes. The zonal-mean wind profiles of the total zonal wind, fixed subtropical jet, and resulting zonal eddy-driven jet are plotted in scaled units (20 m/s $\sim$ 0.15). (d–f) Zonal-mean zonal wind profiles composited when the eddy-driven jet Z_{lat} is equatorward and poleward of 54°N. (g–i) K^* times the radius of the earth composited as in d–f for the vorticity power-weighted phase speed c at the latitude of the jet. The filled circle denotes the latitude of the eddy driven jet.